ARTICLE
Journal of Cellular Biochemistry 116:2504–2516 (2015)

Journal of Cellular Biochemistry

Dissociation of MIF-rpS3 Complex and Sequential NF-κB Activation Is Involved in IR-Induced Metastatic Conversion of NSCLC

HyeSook Youn,[1,2] Beomseok Son,[3] Wanyeon Kim,[1,2] Se Young Jun,[4] Jung Sub Lee,[5] Jae-Myung Lee,[6] ChulHee Kang,[4] Joon Kim,[7] and BuHyun Youn[1,2,3]*

[1]*Department of Biological Sciences, Pusan National University, Busan, 609-735, Republic of Korea*

[2]*Nuclear Science Research Institute, Pusan National University, Busan, 609-735, Republic of Korea*

[3]*Department of Integrated Biological Science, Pusan National University, Busan, 609-735, Republic of Korea*

[4]*Department of Chemistry, Washington State University, Pullman WA 99164, USA*

[5]*Department of Orthopaedic Surgery, Medical Research Institute, Pusan National University School of Medicine, Busan, 602-739, Republic of Korea*

[6]*Department of Naval Architecture and Ocean Engineering, Pusan National University, Busan, 609-735, Republic of Korea*

[7]*Laboratory of Biochemistry, School of Life Sciences & Biotechnology, Korea University, Seoul, 136-701, Republic of Korea*

ABSTRACT

Frequent relapse and spreading of tumors during radiotherapy are principal obstacles to treatment of non-small cell lung cancer (NSCLC). In this study, we aimed to investigate how macrophage migration inhibitory factor (MIF) which is expressed at high levels in metastatic and primary lung cancer cells could regulate NSCLC metastasis in response to ionizing radiation (IR). The results indicated that MIF and ribosomal protein S3 (rpS3) were shown to be connected to inflammation, proliferation, and metastasis of NSCLC via IR-induced activation of the NF-κB pathway. Under unirradiated conditions, MIF physically established a complex with rpS3. MIF-rpS3 dissociation induced by IR activated NF-κB and made the expression of target genes of this factor transactivated in two NSCLC cell lines, A549, and NCI-H358. We also found that IR-induced dissociation of this complex led to increased secretion of pro-inflammatory cytokines and modulated the expression of epithelial–mesenchymal transition marker proteins. Finally, the effects of IR-induced dissociation of the MIF-rpS3 complex on tumor metastasis were confirmed by in vivo xenograft studies. Taken together, the present study revealed that dissociation of the MIF-rpS3 complex and subsequent activation of NF-κB is a critical post-IR exposure event that accounts for IR-induced metastatic conversion of NSCLC. J. Cell. Biochem. 116: 2504–2516, 2015.

KEY WORDS: METASTASIS; MIF; rpS3; NF-κB; NON-SMALL CELL LUNG CANCER

Conflicts of interest: The authors declare no conflicts of interest.

HyeSook Youn and Beomseok Son contributed equally to this work.

Grant sponsor: Ministry of Science, ICT & Future Planning, Republic of Korea; Grant number: 2013M2A2A7042502; Grant sponsor: Ministry of Health & Welfare, Republic of Korea; Grant number: 1320100; Grant sponsor: Ministry of Science, ICT & Future Planning, Republic of Korea; Grant number: 2014R1A1A1A05002112; Grant sponsor: Ministry of Science, ICT & Future Planning, Republic of Korea; Grant number: NRF-2012R1A2A1A01009027; Grant sponsor: Ministry of Education, Republic of Korea; Grant number: 2014R1A1A2004061; Grant sponsor: The Financial Supporting Project of Long-term Overseas Dispatch of PNU's Tenure-track Faculty, 2014 ; Grant sponsor: The 2014 Post-Doc. Development Program of Pusan National University.

*Correspondence to: BuHyun Youn, PhD, Department of Biological Sciences, Pusan National University, Busandaehak-ro 63beon-gil, Geumjeong-gu, Busan 609-735, Republic of Korea.
E-mail: bhyoun72@pusan.ac.kr

Manuscript Received: 22 February 2015; Manuscript Accepted: 14 April 2015

Accepted manuscript online in Wiley Online Library (wileyonlinelibrary.com): 20 April 2015

DOI 10.1002/jcb.25195 • © 2015 Wiley Periodicals, Inc.

Non-small cell lung cancer (NSCLC) has malignant characteristics that range from the formation of quiescent tumors to highly metastatic ones. Currently, medically inoperable cases of NSCLC constitute about 25% of the early stage NSCLC, and this number is expected to increase [Powell et al., 2009]. Radiation therapy in the form of stereotactic body radiation therapy (SBRT) has achieved high local control rates among NSCLC patients that cannot be treated by surgery [Bradley et al., 2010]. The dominant pattern of failure among patients receiving radiation therapy, including SBRT, is the development of distant metastasis, or secondary lung cancer and there is also evidence that overall survival associated with early phase NSCLC treated by radiation therapy alone is highly correlated with the occurrence of metastasis at remote sites [Bradley et al., 2010]. This suggests that the identification of radiation-induced biochemical and cell-biological modifications in NSCLC cells is of paramount importance to prevent metastasis and improve therapeutic outcomes.

Inflammation is a physiological response to cellular and tissue damage, including that induced by radiation. Appropriate responses to injury are tightly regulated through a balance between pro- and anti-inflammatory cytokines or signaling molecules. Continuous expression of inflammatory regulators also affects the extent of tumorigenesis [Grivennikov et al., 2010]. These factors aid inhibition of tumor development by the cellular defense system while promoting cancer malignancy, which further leads to tumor invasion, and metastasis. Conceptually, NF-κB links inflammation, tumorigenesis, and resistance of cancer to radiation [Magne et al., 2006]. It confers resistance of neoplastic cells to various kinds of cell death caused by DNA damage or anticancer drugs and radioresistance, angiogenesis, and tumor cell invasiveness can be regulated by NF-κB [Magne et al., 2006]. Additionally, up-regulation of NF-κB expression after treatment with chemotherapeutic drugs and radiation therapy has recently been reported [Li and Sethi, 2010].

Recent study suggested that macrophage migration inhibitory factor (MIF) may be a key factor in cancer progression, particularly for lung malignancies, and metastasis [Rendon et al., 2007]. The ability of MIF to inhibit anti-inflammatory effects indicates its correlation with malignancy, since chronic inflammation is considered to induce tumor formation and metastasis. Inflammatory cytokines are a part of the host immune system and help maintain physiological states by protecting organs against infection and neoplasms. However, in cases of chronic inflammation, these factors may promote the development of cancer, and metastasis. Moreover, MIF is known to suppress the apoptosis-regulating function of p53 [Bifulco et al., 2008]. Increased secretion of MIF stimulated by monocytes may cause high levels of angiogenesis and tumor metastasis in cases of NSCLC [White et al., 2001] and a recent proteome analysis indicated that MIF is a prospective biomarker of NSCLC [Gamez-Pozo et al., 2012].

Ribosomal protein S3 (rpS3) is a member of the 40S subunit of eukaryotic ribosomes and controls the maturation of ribosomes and translation initiation through cooperation with the eukaryotic initiation factors eIF2 and eIF3 [Schafer et al., 2006]. RpS3 is involved in numerous functions that are irrelevant to ribosomal activities including DNA repair, apoptosis, development, metastasis, and radioresistance [Kim et al., 2009; Jang et al., 2011; Graifer et al., 2014]. In particular, rpS3 is known to act as a non-Rel subunit of the NF-κB complex and to associate with Rel dimers to regulate NF-κB-induced transcriptional activation [Wan et al., 2007]. However, the precise mechanism underlying rpS3 regulation is still unclear. One way to elucidate the functions of rpS3 is to analyze the role of rpS3-interacting proteins that alter rpS3 activity.

Although the mechanism governing the early steps of primary tumor cell dispersion has been studied extensively, the process that leads to metastatic conversion in the presence of stress such as ionizing radiation (IR) delivered during radiotherapy remains obscure. The current study was conducted to elucidate mechanisms that promote IR-induced metastasis of NSCLC cells. We hypothesized that MIF overexpression of lung cancer cells and interaction between MIF and rpS3 are associated with IR-induced metastasis of NSCLC cells. Our findings provide a possible explanation of how the metastatic conversion of NSCLC cells is initiated and regulated in response to irradiation.

MATERIALS AND METHODS

CHEMICALS, ANTIBODIES, AND REAGENTS

4,5,6,7-Tetrabromobenzotriazole (TBB), pyrrolidine dithiocarbamate (PDTC), and TG101209 were obtained from Sigma (St. Louis, MO). Antibodies specific for phosphorylated (p)-Tyr, acetyl-lysine, MIF, glutathione S-transferase (GST), rpS3, Tubulin, p-Ser/Thr, IκBα, p-IκBα, p65, p50, Lamin A/C, IgG, C-X-C chemokine receptor type 4 (CXCR4), interleukin (IL)-1β, IL-6, E-cadherin, Vimentin, and Fibronectin were purchased from Santa Cruz Biotechnology (Santa Cruz, CA) or Cell Signaling Technology (Beverly, MA) for Western blot analysis or immunoprecipitation (IP). Cell culture media (RPMI-1640), FBS, glutamine, penicillin, streptomycin, and Trizol® were obtained from Gibco (Grand Island, NY). SiRNA specific for casein kinase 2α (CK2α) and MIF as well as control siRNA were purchased from Dharmacon (Lafayette, CO).

CELL LINES, CELL CULTURE, IRRADIATION, AND DRUG TREATMENT

A549 and NCI-H358 cells were obtained from the American Type Culture Collection (ATCC, Manassas, VA), authenticated, and maintained in early passages, no more than 6 months after receipt from ATCC. The cells were grown in RPMI-1640 medium consisting of 10% FBS, 100 U/mL penicillin, and 100 μg/mL streptomycin at 37°C in 95% air/5% CO_2. The cells were exposed to a single dose of γ-rays employing a Gamma Cell-40 Exactor (Nordion International, Inc., Kanata, Ontario, Canada) at a dose rate of 0.81 Gy/min. Flasks containing the control cells were put in the irradiation chamber but not irradiated. The cells were treated with the indicated molecule dissolved in dimethyl sulfoxide (DMSO).

WESTERN BLOT ANALYSIS, IP, AND TRANSIENT TRANSFECTION

For Western blot analysis, whole cell lysates (WCL), and cytoplasmic/nuclear extract (CE/NE) were prepared as previously described [Yang et al., 2011]. WCL were extracted using RIPA lysis buffer (50 mM Tris, pH 7.4, 150 mM NaCl, 1% Triton X-100, 25 mM NaF, 1 mM DTT, 20 mM EGTA, 1 mM Na_3VO_4, 0.3 mM PMSF, and 5 U/mL Aprotinin)

and the protein concentration of the lysates was verified using a Bio-Rad protein assay kit (Bio-Rad Laboratories, Hercules, CA). To prepare the CE/NE, cells were suspended in buffer A (10 mM HEPES, pH 7.9, 50 mM NaCl, 1 mM DTT, 0.1 mM EDTA, 1 mM PMSF, 1 μg/mL Aprotinin, 5 μg/mL Leupeptin, and 1 μg/mL Pepstatin A) and then incubated for 20 min on ice. An equal volume of buffer B (buffer A + 0.1% NP-40) was then added and the cells were incubated for 20 min on ice. Next, the samples were centrifuged at 5,000 *g* for 2 min to remove cellular debris and the CE was collected. The resulting nuclear pellet was washed twice with buffer A and then resuspended using buffer C (10 mM HEPES, pH 7.9, 400 mM NaCl, 1 mM DTT, 1 mM EDTA, and 1 mM EGTA). The NE was prepared by centrifugation at 13,000 rpm and 4°C for 15 min to remove the cellular debris. Samples were then separated by SDS-PAGE, transferred to a nitrocellulose membrane, and blocked with 5% skim milk in TBS with Tween 20 (10 mM Tris, 100 mM NaCl, and 0.1% Tween 20) for 30 min at room temperature. The membranes were subsequently probed using specific primary antibodies and peroxidase-conjugated secondary antibody (Santa Cruz Biotechnology). Antibody binding was visualized using an enhanced chemiluminescence detection system (Roche Applied Science, Penzberg, Germany).

IP studies were performed as previously described [Kim et al., 2010]. For transient transfection, cells were plated at a density of 5×10^5 cells in 6-well dishes and then incubated for 4 h. Next, the cells were transiently transfected with the indicated plasmid using Lipofectin (Invitrogen, Carlsbad, CA) or the siRNA oligonucleotides (10 nM) using DharmaFECT 1 from Dharmacon (Lafayette, CO) according to the manufacturers' instructions.

IN VITRO PULL-DOWN ASSAY

Prepared His-MIF- or His-rpS3-bound resin was incubated at 4°C for 6 h with 10 μg of purified GST-rpS3 or GST-MIF, respectively, in 100 μL of binding buffer (20 mM Tris-HCl, pH 7.9, 100 mM KCl, 2.5 mM $CaCl_2$, 2.5 mM $MgCl_2$, 1 mM DTT, and 0.1% Triton X-100). After a brief centrifugation, the beads were washed three times with washing buffer (50 mM imidazole, 500 mM NaCl, and 20 mM Tris-HCl, pH 7.9) and resuspended in elution buffer (1 M imidazole, 500 mM NaCl, and 20 mM Tris-HCl, pH 7.9). The samples were subjected to SDS-PAGE and immunoblotting with a primary anti-GST antibody and a peroxidase-conjugated secondary antibody.

ISOTHERMAL TITRATION CALORIMETRY (ITC) ASSAY

Protein–protein interaction was characterized by titrating protein ligand (rpS3 or lysozyme) into a protein solution (MIF) and measuring the changes in binding thermodynamics with a VP-ITC calorimeter (Microcal Inc., Northampton, MA) as previously described [Kim et al., 2013]. Both His-rpS3 (or lysozyme) and His-MIF samples were exhaustively dialyzed under similar buffer conditions with 20 mM Tris/HCl (pH 7.5), 50 mM $(NH_4)_2SO_4$, 1 mM TCEP, and 5 mM $CaCl_2$. To ensure that the protein samples were devoid of air bubbles prior to the experiment, samples were centrifuged, and degassed under vacuum. Titrations were performed by injecting 10 μL aliquots of rpS3 (or lysozyme; 1 mM) as a protein ligand (29 injections) into 0.1 mM of MIF protein. The injections were made over a period of 20 s with a 240-s interval between subsequent injections. The sample cell with a 1.4 mL capacity was stirred at 310 rpm. The experiments were conducted at 25°C with heat change accompanying every injection being monitored. The protein ligand–protein titration curves were corrected using protein-to-buffer control titration and analyzed using Origin7.0 software supplied by Microcal, Inc.

BIMOLECULAR FLUORESCENCE COMPLEMENTATION (BIFC) ASSAY

pBiFC-EGFR-VN and pBiFC-EGFR-VC constructs were kindly provided by Dr. Chang-Deng Hu (Purdue University, West Lafayette, IN) and Dr. Ichi N. Maruyama (Okinawa Institute of Science and Technology Graduate University, Okinawa, Japan). To construct pBiFC-MIF-VN, a MIF-encoding DNA fragment was amplified by PCR and then inserted into the *Kpn*I site of pBiFC-EGFR-VN, where the region encoding EGFR had been located. To construct pBiFC-rpS3-VC, a DNA fragment encoding rpS3 was amplified, and inserted between the *Sal*I and *Xho*I sites of pBiFC-EGFR-VC, eliminating the EGFR DNA fragment. A549 or NCI-358 cells were transiently transfected with pBiFC-MIF-VN and pBiFC-rpS3-VC and fluorescence was detected with an Olympus IX71 fluorescence microscope (Olympus Optical Co. Ltd., Tokyo, Japan).

LUCIFERASE REPORTER GENE ASSAY

A luciferase assay was performed as previously described [Yang et al., 2013].

CHROMATIN IMMUNOPRECIPITATION (CHIP) ASSAY

A ChIP assay was performed as previously described [Kim et al., 2011]. PCR was performed with primers specific for human *IL8*, *NFKBIA*, *CXCR4*, *IL1B*, *IL6,* and *ACTB* promoters (Supplementary Table S1).

REAL-TIME QUANTITATIVE RT-PCR (QRT-PCR)

The level of pro-inflammatory and epithelial–mesenchymal transition (EMT)-related gene expression was measured using qRT-PCR as previously described [Kang et al., 2013]. Aliquots of a master mix containing all of the reaction components with the primers (Supplementary Table S2) were dispensed into a real time PCR plate (Applied Biosystems, Foster City, CA). All of the PCR reagents were from a SYBR Green core reagent kit (Applied Biosystems). Expression of all genes evaluated was measured in triplicate in the reaction plate. qRT-PCR was performed using an Applied Biosystems-7900 HT qRT-PCR instrument. PCR was performed for 40 cycles of 95°C for 15 s and 60°C for 1 min followed by thermal denaturation. The expression of each gene relative to that of *GAPDH* mRNA was determined using the $2^{-\Delta CT}$ method. To simplify data presentation, the relative expression values were multiplied by 10^2.

CONCENTRATION OF MEDIA AND COOMASSIE BLUE STAINING

A549 or NCI-H358 cells were grown to confluence in RPMI containing 10% FBS. The media were then collected and at 2,000*g* and 4°C for 10 min. The supernatant was concentrated fivefold with Amicon Ultracell 10K filters (Millipore, Billerica, MA) and proteins in the concentrated media were subjected to SDS-PAGE. Western blotting was performed as described above. To verify equal loading, sample-loaded gels were stained using 0.25% Coomassie brilliant

blue R-250 (Sigma), and then destained in methanol: acetic acid: distilled water (3:1:6) solution.

CYTOKINE-SPECIFIC ENZYME-LINKED IMMUNOSORBENT ASSAY (ELISA)

Cells (8×10^5) were plated in 6-well plates and grown to 80% confluence. Following the desired treatments, the amounts of IL-1β and IL-6 released into the media were measured using ELISA kits (R&D Systems, Abingdon, UK) according to the manufacturer's instructions.

CELL ASSAY (3D CULTURE) AND IMMUNOFLUORESCENCE (IF) STAINING

The 3D culture and IF staining were performed as previously described [Kim et al., 2014].

TRANSWELL CELL MIGRATION ASSAY

To measure the migration capacity of NSCLC cells, a transwell cell migration assay was conducted as previously described [Kang et al., 2013].

WOUND HEALING ASSAY

Monolayers of cells were scratched using a 200-μL pipette tip after the cells had reached 70% confluency in RPMI-1640 medium supplemented with 1% FBS. The cells were then incubated with fresh medium with or without treatment for 19 h. Photomicrographs were taken at 100× magnification using an Olympus IX71 fluorescence microscope (Olympus Optical Co. Ltd.).

ANIMAL CARE PROTOCOL AND TUMOR XENOGRAFT IN NUDE MICE

Six-week-old male BALB/c athymic nude mice (Central Lab Animals Inc., Seoul, Republic of Korea) were used for in vivo experiments. The protocols used were approved by the Institutional Animal Care and Use Committee of Pusan National University (Busan, Republic of Korea), and performed in accordance with provisions of the NIH Guide for the Care and Use of Laboratory Animals. The mice were housed individually or in groups of up to five in sterile cages. They were maintained in animal care facilities in a temperature-regulated room (23 ± 1°C) with a 12 h light/dark cycle and quarantined for 1 week prior to the study. All animals were fed water and a standard mouse chow ad libitum. Mice (n = 3 per group) were injected with 2×10^6 A549 or NCI-H358 cells in the flank and tumors were allowed to develop. Upon identification of a palpable tumor (minimum volume of 200 mm^3), DMSO or drug (200 μg/kg body weight) was administered intraperitoneally every day for 30 days. The animals were also irradiated with 10 Gy once a week for 4 week. Tumor length (L) and width (l) were measured with a caliper and tumor volumes were calculated with the formula $(L \times l^2)/2$. At the end of the treatment period, animals were euthanized, and the tumors were harvested, homogenized, and processed for Western blotting.

STATISTICAL ANALYSIS

All numeric data are presented as the mean ± standard error of the mean from at least three independent experiments. The results were analyzed using a one-way ANOVA on ranked data followed by a Tukey's honestly significant difference test, and a two-way ANOVA on ranked data followed by a Bonferroni post test. Prism 5 software (GraphPad Software, San Diego, CA) was used to conduct all statistical analyses. A P-value <0.05 was considered statistically significant.

RESULTS

MIF INTERACTS WITH rpS3 IN VITRO AND IN VIVO

To identify the factors and mechanisms that govern metastatic conversion of NSCLC cells in response to irradiation, we analyzed multiple datasets of human lung cancer using the Oncomine database (http://www.oncomine.org). Among several genes greatly overexpressed in lung cancer cells, we focused on the *MIF* gene based on its high expression in these cells (Fig. 1A) [Landi et al., 2008; Hou et al., 2010]. Datasets available from Oncomine also demonstrated that metastatic lung cancer cells and primary lung cancer cells contained high levels of MIF (Supplementary Fig. S1). Consistent with previous studies [Landi et al., 2008; Hou et al., 2010], we observed that MIF is significantly overexpressed in cases of human lung adenocarcinoma (or NSCLC cells), but was not expressed in normal lung tissues or cells (data not shown). These findings led us to hypothesize that MIF overexpression might be associated with both lung tumor malignancy and metastatic conversion. Therefore, we investigated whether post-translational modification of MIF contributes to metastatic conversion of lung cancer cells under IR stress, a potent inducer of metastasis. Post-translational alteration may enable the biological functions of several biomarkers for metastatic conversion of some cancer types [Leeming et al., 2011]. IR-dependent molecular modification of MIF was investigated since MIF is known to be phosphorylated (Y37) or acetylated (K78) [Choudhary et al., 2009; Moritz et al., 2010]. However, IR-induced MIF phosphorylation or acetylation was not observed in either A549 or NCI-H358 cells (Fig. 1B).

We next investigated biochemical and dynamic activities of MIF. Based on our previous yeast two-hybrid analysis, MIF was selected as an rpS3-interacting candidate [Kim et al., 2013]. Given the multi-functional and regulatory activities of rpS3 in cancer cells and biochemical relationships with various binding partners [Graifer et al., 2014], we hypothesized that the association of MIF and rpS3 could functionally influence the metastasis of NSCLC cells. We evaluated the interaction of MIF with rpS3 using an in vitro pull-down assay, and confirmed that MIF and rpS3 could bind to each other (Fig. 1C). The interaction of MIF (or rpS3) with endogenous rpS3 (or MIF) was also detected in NSCLC cells (Fig. 1D). Furthermore, an ITC experiment was conducted to assess the thermodynamics of the MIF-rpS3 interaction. Calorimetric data revealed that heat was released when rpS3 was associated with MIF, indicating a significant enthalpic contribution to the MIF-rpS3 interaction ($K_d = 16.0$ μM, $\Delta H = -23.7 \pm 1.8$ kcal/mol, $\Delta S = -16.3$ cal/mol degree; Fig. 1E). The ITC data showed that rpS3 binds to MIF with a stoichiometry of 1:1.

To determine the subcellular localization and kinetics in association between MIF and rpS3, a BiFC assay was performed using A549 or NCI-H358 cells transfected with expression vectors encoding N-terminal Venus bound to MIF (pBiFC-MIF-VN) and C-terminal Venus-conjugated rpS3 (pBiFC-rpS3-VC). Data from the

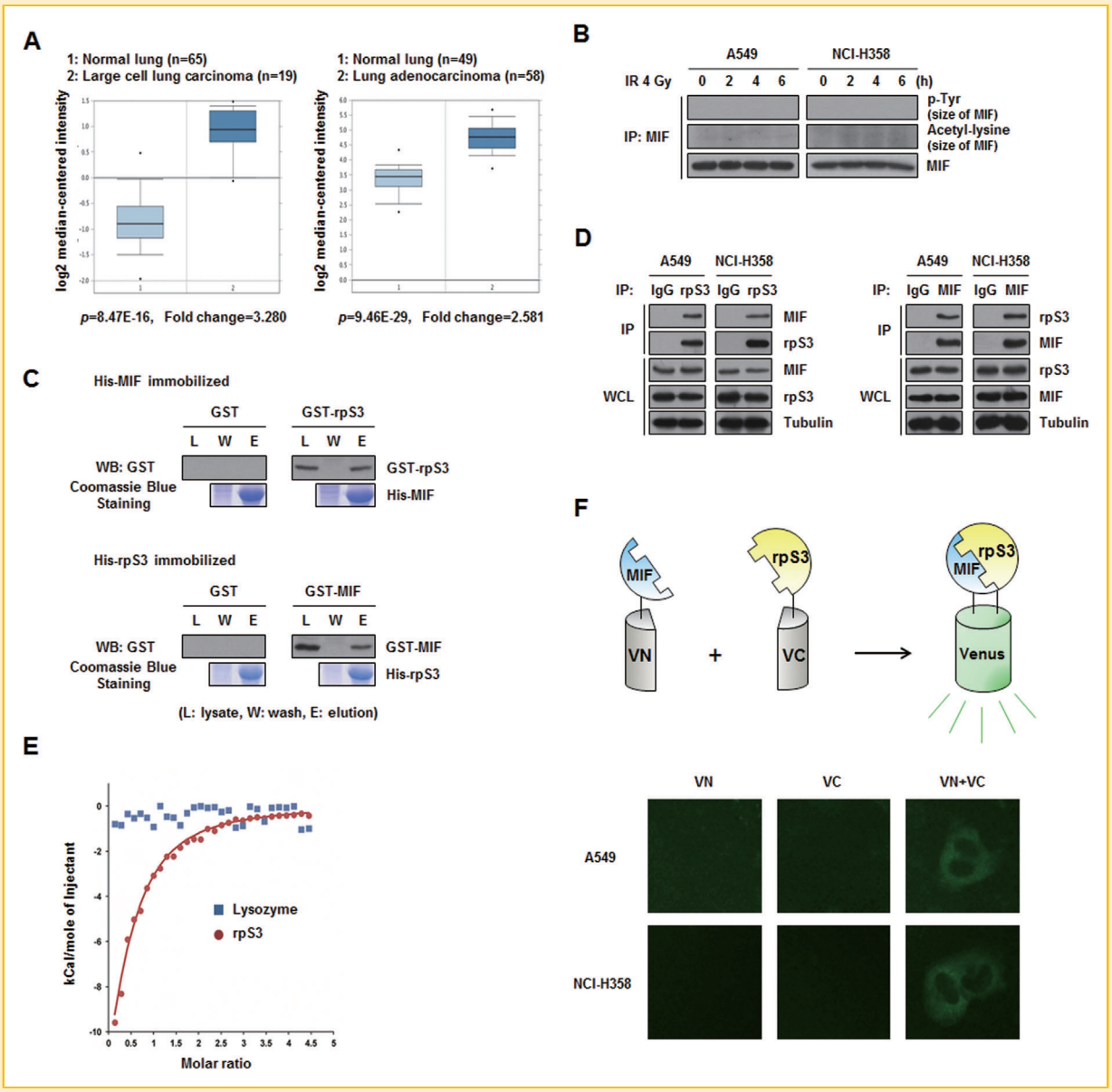

Fig. 1. MIF can physically associate with rpS3. (A) Expression of the *MIF* gene in normal lung and lung cancer tissues was evaluated with data from the Oncomine database (http://www.oncomine.org). Left [Hou et al., 2010]; $P = 8.47 \times 10^{-16}$, Fold change = 3.280. Right [Landi et al., 2008]; $P = 9.46 \times 10^{-29}$, Fold change = 2.581. (B) Post-translational modifications of MIF in response to IR were assessed. The cells were harvested 0, 2, 4, or 6 h after 4 Gy of irradiation. Cell lysates were immunoprecipitated with an anti-MIF antibody and subjected to Western blot analysis for p-Tyr and acetyl-lysine. (C) A GST pull-down assay was used to verify in vitro binding of MIF to rpS3. Coomassie blue staining showed that equal amounts of His-fused proteins were used. (D) MIF-rpS3 interaction in A549 and NCI-H358 cells was monitored by a reciprocal IP assay. After preparation of cell extract, lysates were subjected to an IP assay with an anti-rpS3 antibody or anti-MIF antibody followed by Western blot analysis. (E) Significant interaction between MIF and rpS3 was revealed based on ITC data. Heat of injection was experimentally determined during titration of MIF in the presence of rpS3 (●) or Lysozyme (■). Solid lines represent the least square fits of the data using a one-site binding model. Lysozymes not known to interact with MIF did not show any significant binding to MIF. (F) A BiFC assay was performed to determine the interaction of MIF-rpS3 in live cells. A scheme of the BiFC assay is presented (upper panel). Cells were transiently transfected with pBiFC-MIF-VN and/or pBiFC-rpS3-VC. Fluorescence indicative of MIF-rpS3 binding was only observed when both MIF-VN and rpS3-VC were present (lower panel).

BiFC assay provide evidence of interactions between two proteins that can be detected by fluorescence in live cells (Fig. 1F, upper panel). Fluorescence was observed in cells expressing both pBiFC-MIF-VN and pBiFC-rpS3-VC, but not in those that solely expressed pBiFC-MIF-VN or pBiFC-rpS3-VC (Fig. 1F, lower panel). Taken together, these results indicate that MIF physically associates with rpS3 in vitro and in vivo in NSCLC cells.

IR INDUCES CK2α-MEDIATED PHOSPHORYLATION OF rpS3 AND DISSOCIATION OF THE MIF-rpS3 COMPLEX

Since MIF and rpS3 interacted with each other under unirradiated conditions, we subsequently monitored IR-induced biochemical changes of MIF and rpS3. Interestingly, MIF was not able to form a complex with rpS3 in irradiated A549 and NCI-H358 cells (Fig. 2A). In contrast, MIF-rpS3 complex formation was detected under

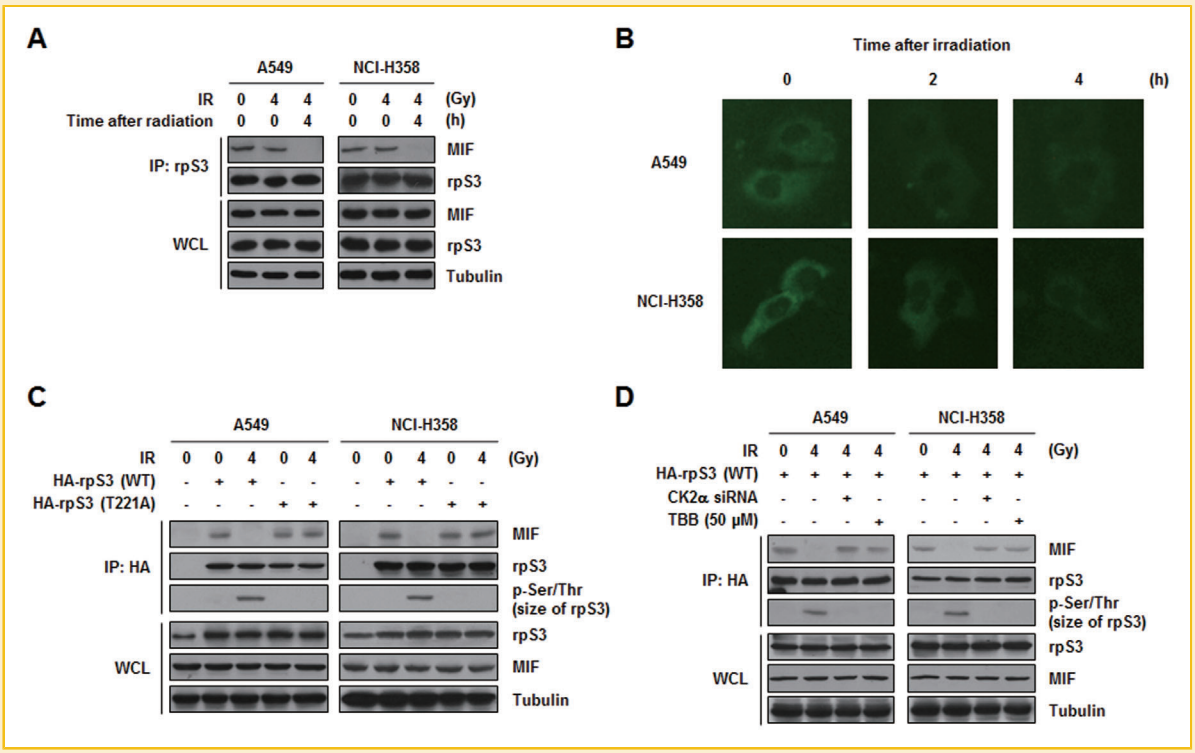

Fig. 2. RpS3 phosphorylation by CK2α induces the loss of MIF–rpS3 interaction in response to IR. (A) MIF–rpS3 interaction with IR was measured in NSCLC cell lines by an IP assay using an anti-rpS3 antibody. Cell lysates were prepared 4 h after irradiation, immunoprecipitated with an anti-rpS3 antibody and subjected to Western blot analysis using an anti-MIF antibody. (B) The interaction between MIF and rpS3 in live cells was observed by BiFC analysis. Cells transfected with pBiFC-MIF-VN and pBiFC-rpS3-VC were monitored 0, 2, or 4 h after irradiation (4 Gy) using a fluorescence microscope. (C) The effect of Thr221 phosphorylation of rpS3 on IR-induced dissociation of the MIF–rpS3 complex was investigated using a T221A mutant of rpS3. After irradiation, cell lysates were immunoprecipitated with an anti-HA antibody followed by Western blot analysis for MIF. (D) The influence of CK2α siRNA or TBB (50 μM) on dissociation of the MIF–rpS3 complex resulting from IR was investigated. Cells treated with CK2α siRNA or TBB were irradiated and the phosphorylation state of rpS3 was assessed.

unirradiated conditions as shown in Figure 1D. In the BiFC assay, fluorescence intensity decreased in a time-dependent manner in response to 4 Gy of IR (Fig. 2B). This finding suggests that the interaction between MIF and rpS3 was reduced due to IR exposure.

Our previous study demonstrated that rpS3 is phosphorylated by IR-activated CK2α at Thr-221 in NSCLC cells [Kim et al., 2013]. Accordingly, we investigated whether or not rpS3 phosphorylation actually influences IR-dependent dissociation of the MIF-rpS3 complex. We found that phosphorylation of rpS3 at Thr221 is required for IR-dependent MIF-rpS3 dissociation in NSCLC cells (Fig. 2C). IR-induced dissociation of the MIF-rpS3 complex was not observed in the presence of CK2α siRNA or a CK2α inhibitor, TBB, in irradiated NSCLC cells (Fig. 2D). Taken together, these results indicate that the MIF-rpS3 complex cannot be established when rpS3 is phosphorylated by IR-activated CK2α.

DISSOCIATED rpS3 AND MIF ACCELERATE ACTIVATION OF THE NF-κB PATHWAY IN RESPONSE TO IR

Following analysis of the dynamic interaction between MIF and rpS3 upon irradiation, the effect of dissociated rpS3 on metastatic conversion was investigated. NF-κB has been reported to increase tumor-associated inflammation that promotes metastasis [Ben-Neriah and Karin, 2011]. In addition, rpS3 was shown to be involved in the development of radioresistance through NF-κB activation in irradiated NSCLC cells [Kim et al., 2013]. Therefore, we evaluated the relationship between dissociated rpS3 and activation of the NF-κB pathway in NSCLC cells. As shown in Figure 3A,B, IR increased IκBα phosphorylation, nuclear translocation of p65, and NF-κB transcriptional activation in NSCLC cells. These modifications were significantly attenuated by inhibition of MIF-rpS3 complex dissociation via CK2α siRNA treatment. Furthermore, Thr221 phosphorylation-dependent nucleus localized rpS3 bound NF-κB complex (p65 and p50) in irradiated NSCLC cells (Fig. 3C). These results indicate that activation of the NF-κB pathway in NSCLC cells is intimately linked with the free form of phosphorylated rpS3 in the presence of IR.

Next, we conducted a ChIP assay to verify the link between dissociated rpS3 and NF-κB activation. We focused on specific NF-κB binding sites within the promoters of *IL8* and *NFKBIA* that are well-known NF-κB target genes. Compared to HA-rpS3 (wild-type, WT), transfection with HA-rpS3 (T221A) caused a significant decrease in the recruitment of rpS3 and p65 to the *IL8* and *NFKBIA* promoter regions (Fig. 3D). Therefore, our data suggest that a significant increase in NF-κB transcriptional activation in NSCLC cells could be facilitated by elevating the DNA binding property of p65 through IR-induced binding of phosphorylated rpS3 with the p65 subunit of the NF-κB complex.

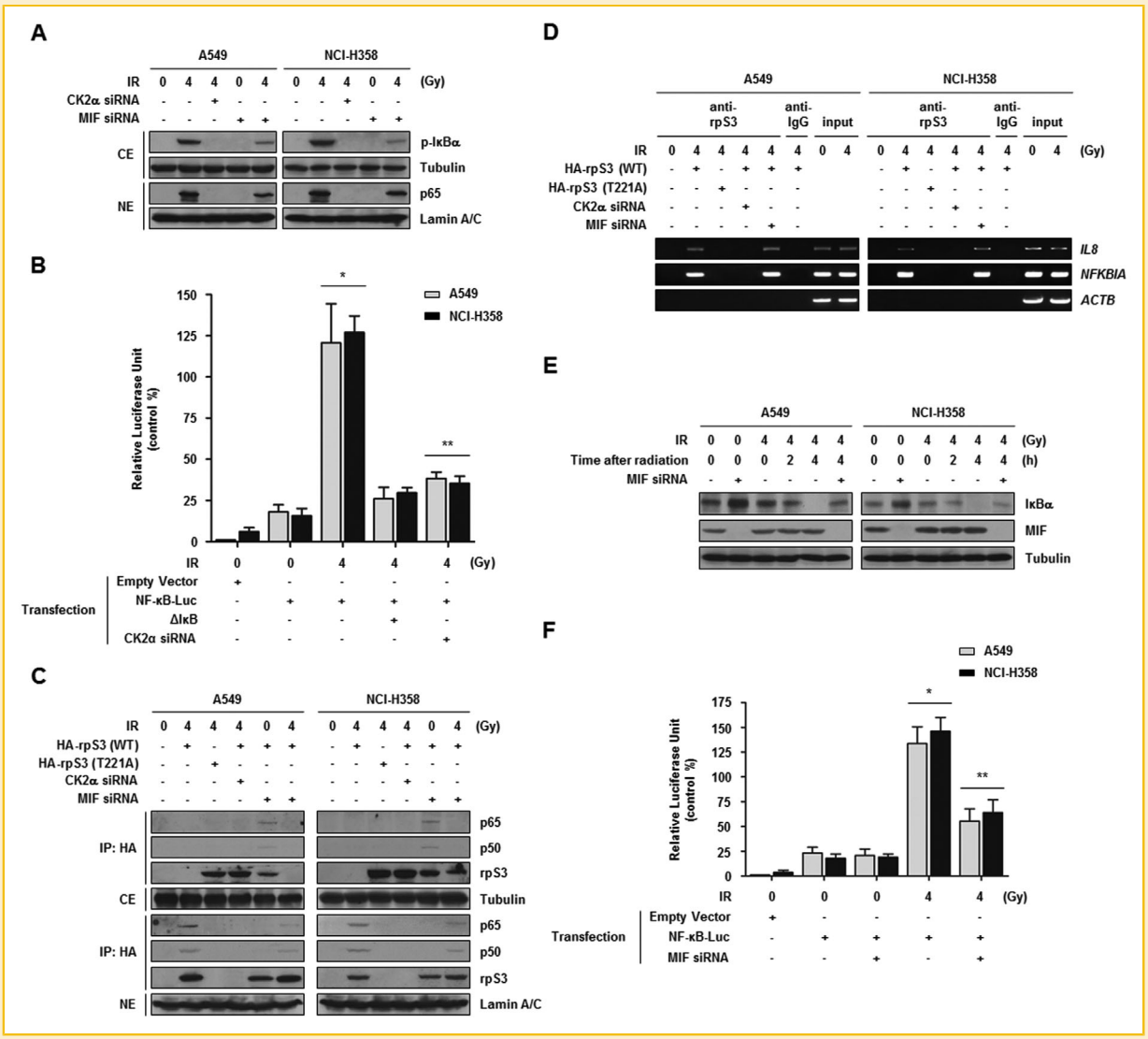

Fig. 3. Dissociated rpS3 and MIF activate NF-κB. (A) The effects of IR on NF-κB (p65) activation along with the impact of CK2α siRNA or MIF siRNA were measured. After the indicated treatment, cell lysates were subjected to Western blot analysis using anti-p-IκBα and anti-p65 antibodies. Tubulin and Lamin A/C were used as loading controls for the cytoplasmic extracts (CE) and nuclear extracts (NE), respectively. (B) Increased transcriptional activation of NF-κB caused by IR was measured by a luciferase reporter gene assay. $^{*}P < 0.05$ compared with non-irradiated cells; $^{**}P < 0.05$ compared with irradiated cells. (C) IR-induced interaction of rpS3 with NF-κB (p65 and p50) in the nucleus was measured by an IP assay after cytoplasmic/nuclear fractionation. Following treatment with each siRNA and irradiation, each lysate was immunoprecipitated with an anti-HA antibody and then subjected to Western blot analysis using anti-p65 and anti-p50 antibodies. (D) Recruitment of rpS3 to the promoters of *IL8* and *NFKBIA* which are two noted target genes of NF-κB was measured by a ChIP assay. Co-transfected cells were harvested 4 h after irradiation. Chromatin-bound DNA was immunoprecipitated with an anti-rpS3 antibody. (E) The effects of MIF and IR on IκBα expression in A549 and NCI-H358 cells were measured. The cells were harvested 0, 2, or 4 h after irradiation and cell lysates were subjected to Western blot analysis using an anti-IκBα antibody. (F) Results of a reporter gene assay showed that the increase in NF-κB activation in response to IR was diminished by MIF siRNA. $^{*}P < 0.05$ compared with non-irradiated cells; $^{**}P < 0.05$ compared with irradiated cells.

The effect of dissociated MIF on metastatic conversion was then investigated. As shown in Figure 3A,C, the degree of NF-κB activation induced by IR was diminished by treatment with MIF siRNA. These results suggested a possible involvement of MIF in NF-κB activation independently or synergistically with rpS3. Therefore, we examined the relationship of dissociated MIF with activation of the NF-κB pathway in response to IR. As shown in Figure 3E, IR decreased the level of IκBα in a time-dependent manner. This reduction was reversed by treatment with MIF siRNA. Under unirradiated conditions, MIF siRNA increased the level of IκBα. Consistent with the results shown in Figure 3E, effects of MIF on NF-κB activation were confirmed by a reporter gene assay in NSCLC cells (Fig. 3F). These results suggest that dissociation of MIF from rpS3 activates the NF-κB pathway by augmenting the level of free rpS3 and antagonizing IκBα expression resulting from IR exposure in NSCLC cells.

rpS3 AND MIF INDUCE CANCER-ASSOCIATED INFLAMMATION IN RESPONSE TO IR

We next examined IR-induced transcriptional alterations of *CXCR4*, *IL1B*, and *IL6*, which are pro-inflammatory genes regulated by

NF-κB. Significant reductions of *CXCR4*, *IL1B*, and *IL6* mRNA levels were observed in NSCLC cells that had been treated with CK2α siRNA or TBB followed by irradiation (Fig. 4A). Concomitantly, production of cellular CXCR4 and the secreted active forms of IL-1β and IL-6 were reduced by down-regulated CK2α (Fig. 4B). Under the same conditions, reduced secretion of both IL-1β and IL-6 was verified by an ELISA assay (Fig. 4C). In addition, cells were treated with 20 μM PDTC, an NF-κB inhibitor, to determine whether NF-κB directly affects pro-inflammatory pathways activated by irradiation. IR-induced expression of the three inflammation-associated genes was diminished by PDTC treatment (Fig. 4A-C). To verify the direct association between NF-κB and expression profiles of the pro-inflammatory genes, we conducted an additional ChIP assay. When compared to treatment with IR alone, addition of CK2α siRNA or TBB caused a significant decrease in the recruitment of p65 to the promoter regions of *CXCR4*, *IL1B*, and *IL6* (Fig. 4D). Therefore, dissociation of MIF and rpS3 facilitated by CK2α elevates the expression of pro-inflammatory genes through enhanced NF-κB binding to the promoters.

rpS3 AND MIF PROMOTE THE METASTASIS OF NSCLC CELLS UNDER IRRADIATED CONDITIONS

Several lines of evidence have shown that NF-κB and inflammation influence metastasis [Bollrath and Greten, 2009; Gyrd-Hansen and Meier, 2010]. To explore potential effects of the free form of rpS3 and MIF on inflammation-mediated metastatic conversion and those of a CK2α inhibitor as a metastasis suppressor, we monitored morphologic changes of NSCLC cells. The 3D culture model has been used extensively to identify morphological modifications that are distinct features of cancer growth [Debnath and Brugge, 2005; Kim et al., 2014]. In this system, IR-treated NSCLC cells could be distinguished from the control cells and formed an increased number of acini that invaded the Matrigel 3D matrix. However, the observed morphologic changes of the epithelial acini were abrogated upon treatment with TBB, indicating that inhibition of rpS3 phosphorylation by CK2α in the NSCLC cells reduced the IR-dependent EMT (Fig. 5A).

The migration capacity and EMT marker expression of NSCLC cells treated with the CK2α inhibitor were then measured. NSCLC cells treated with 50 μM of TBB had reduced motility as determined by both the transwell cell migration and wound healing assays (Fig. 5B,C). A Janus kinase 2 inhibitor, TG101209, was administered as a positive control of EMT inhibitors [Kim et al., 2014]. TBB treatment prevented IR-induced EMT through increasing the expression of E-cadherin (an epithelial marker) while decreasing the expression of Vimentin and Fibronectin (two mesenchymal markers) at both the mRNA and protein levels (Fig. 5D,E). Consequently, our results suggested that the inhibition of MIF-rpS3 dissociation in NSCLC cells suppressed IR-induced metastatic conversion.

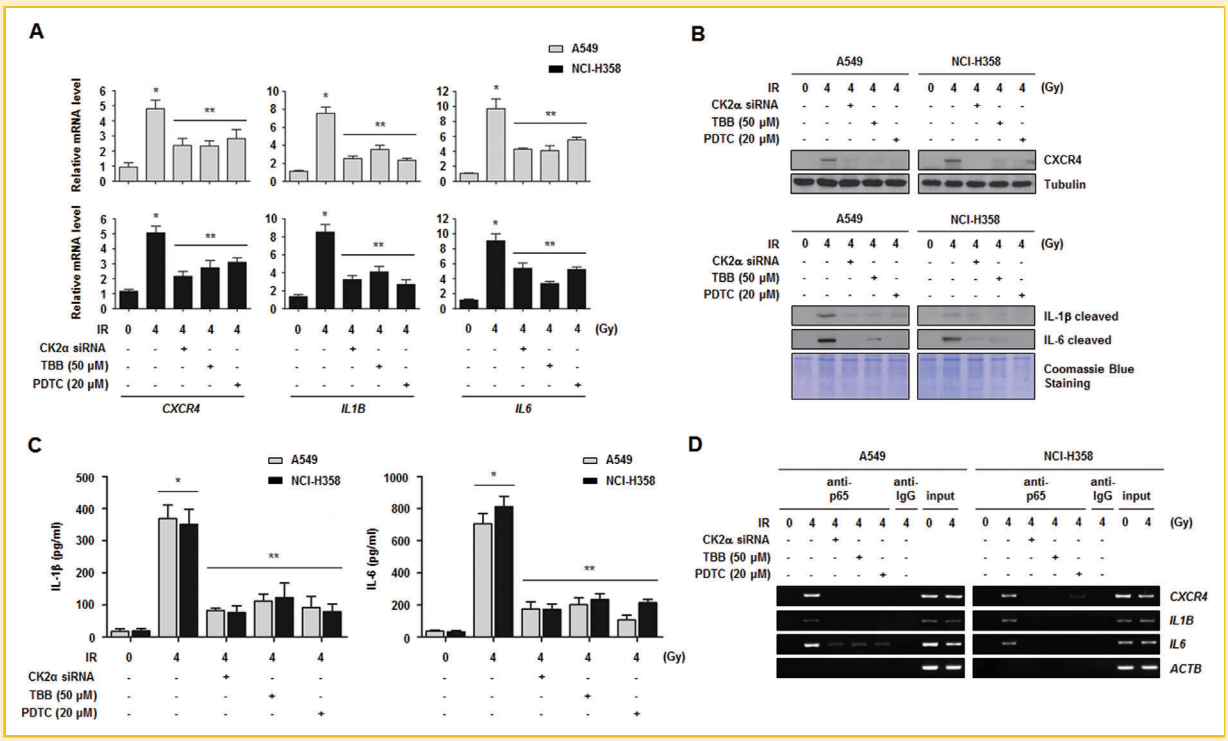

Fig. 4. Dissociated rpS3 and MIF contribute to NF-κB-dependent expression of *CXCR4*, *IL1B*, and *IL6*. (A) The impact of CK2α siRNA, TBB, or PDTC on increased mRNA levels of *CXCR4*, *IL1B*, and *IL6* in response to IR was examined by qRT-PCR. $^{*}P < 0.05$ compared with non-irradiated cells; $^{**}P < 0.05$ compared with irradiated cells. (B) Post-irradiation changes in protein expression of CXCR4, IL-1β, and IL-6 were measured by Western blot analysis. After the indicated treatment, cell lysates and 5-fold concentrated media were subjected to Western blot analysis using specific antibodies. Coomassie blue staining showed equal loading of each sample. (C) Decreased IL-1β and IL-6 secretion after treatment with CK2α siRNA, TBB, or PDTC was demonstrated by an ELISA in NSCLC cells exposed to 4 Gy of IR. $^{*}P < 0.05$ compared with non-irradiated cells; $^{**}P < 0.05$ compared with irradiated cells. (D) Binding of p65 to the promoters of *CXCR4*, *IL1B*, and *IL6* was monitored by a ChIP assay. Co-transfected cells were harvested 4 h after irradiation. Chromatin-bound DNA was immunoprecipitated with an anti-p65 antibody.

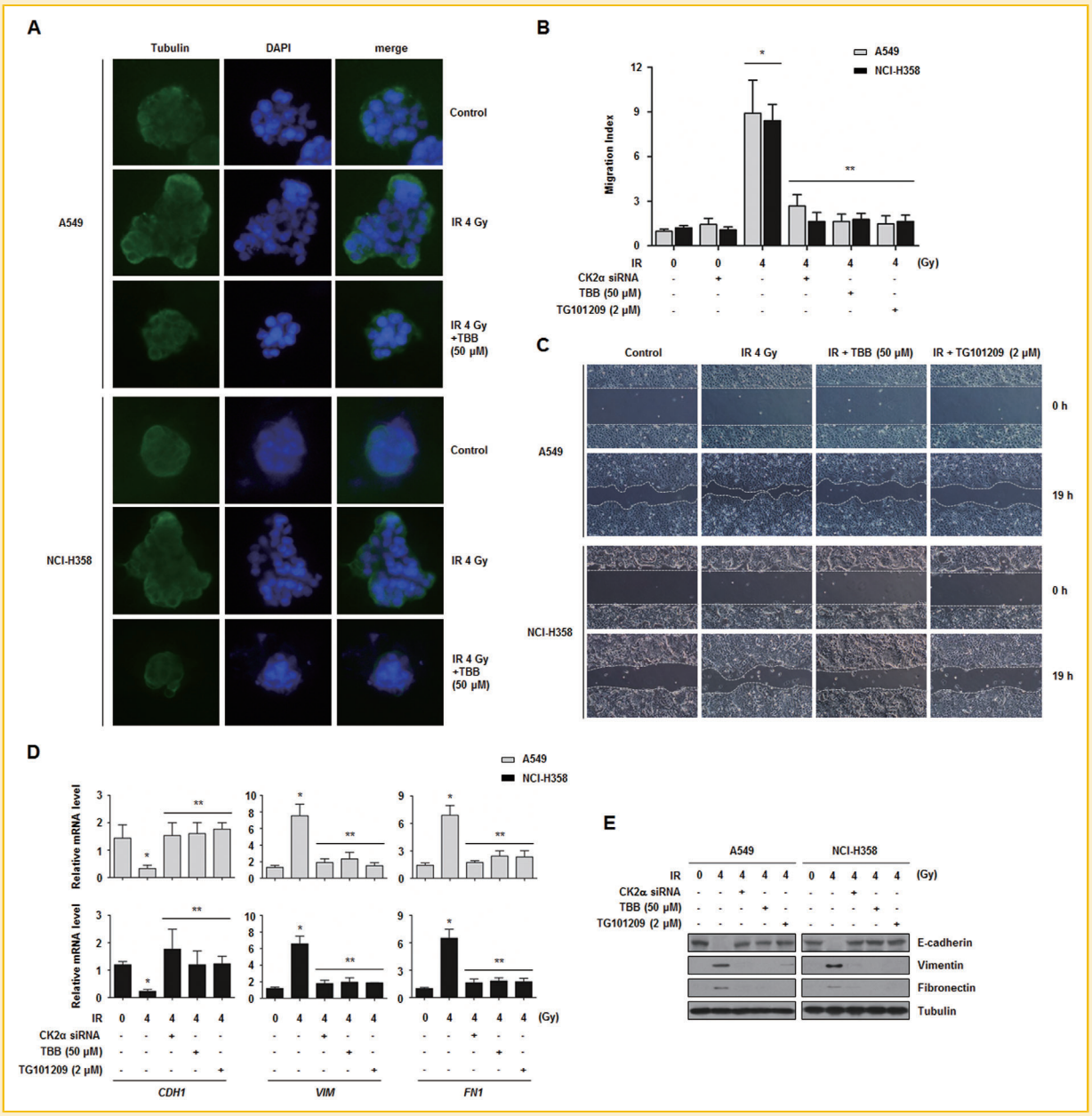

Fig. 5. RpS3 and MIF make NSCLC cells metastatic in response to IR. (A) Morphologic changes of NSCLC cells treated with a CK2α inhibitor were monitored with a 3D culture model. Cells with the indicated treatments were grown on Matrigel and fixed. The cells were then permeabilized and immunostained for Tubulin (green) and with DAPI (blue). (B) The effects of CK2α inhibition on the migration capacity of irradiated cells was measured by a Transwell cell migration assay. Fold-increase of migration compared to the control group is presented based on the relative number of cells in a randomly selected field from three independent experiments. TG101209 was used as a positive control for EMT inhibition. $^{*}P < 0.05$ compared with non-irradiated cells; $^{**}P < 0.05$ compared with irradiated cells. (C) The effects of CK2α inhibition on the migration capacity of irradiated cells were measured by a wound healing assay. Following treatment with TBB and irradiation, cells were wounded and incubated for 19 h. (D) The effects of CK2α inhibition on mRNA expression of *CDH1*, *VIM*, and *FN1* in irradiated NSCLC cells were analyzed by qRT-PCR. $^{*}P < 0.05$ compared with non-irradiated cells; $^{**}P < 0.05$ compared with irradiated cells. (E) The effects of CK2α inhibition on protein expression of E-cadherin, Vimentin, and Fibronectin in irradiated NSCLC cells were analyzed by Western blot analysis using specific antibodies.

IMPEDING DISSOCIATION OF THE MIF-rpS3 COMPLEX UNDER IRRADIATED CONDITIONS DECREASED IR-INDUCED IN VIVO TUMOR METASTASIS AND INCREASED IN VIVO RADIOSENSITIZATION

The properties of EMT have been reported to be highly correlated with proliferation of irradiated NSCLC cells [Kim et al., 2014]. To evaluate combined effects of CK2α inhibition with radiation on tumor growth in vivo, mouse xenograft models were established (Fig. 6A). Radiation (10 Gy) was delivered to BALB/c athymic nude mice once a week for 4 week and DMSO or TBB was administered intraperitoneally every day for 30 d. In vivo data from nude mice bearing tumors formed by A549 and NCI-H358 cells indicated that TBB conferred in vivo radiosensitization (Fig. 6B). The tumor volumes of mice treated with radiation and TBB were significantly reduced by approximately 51.5% (for the group with tumors formed

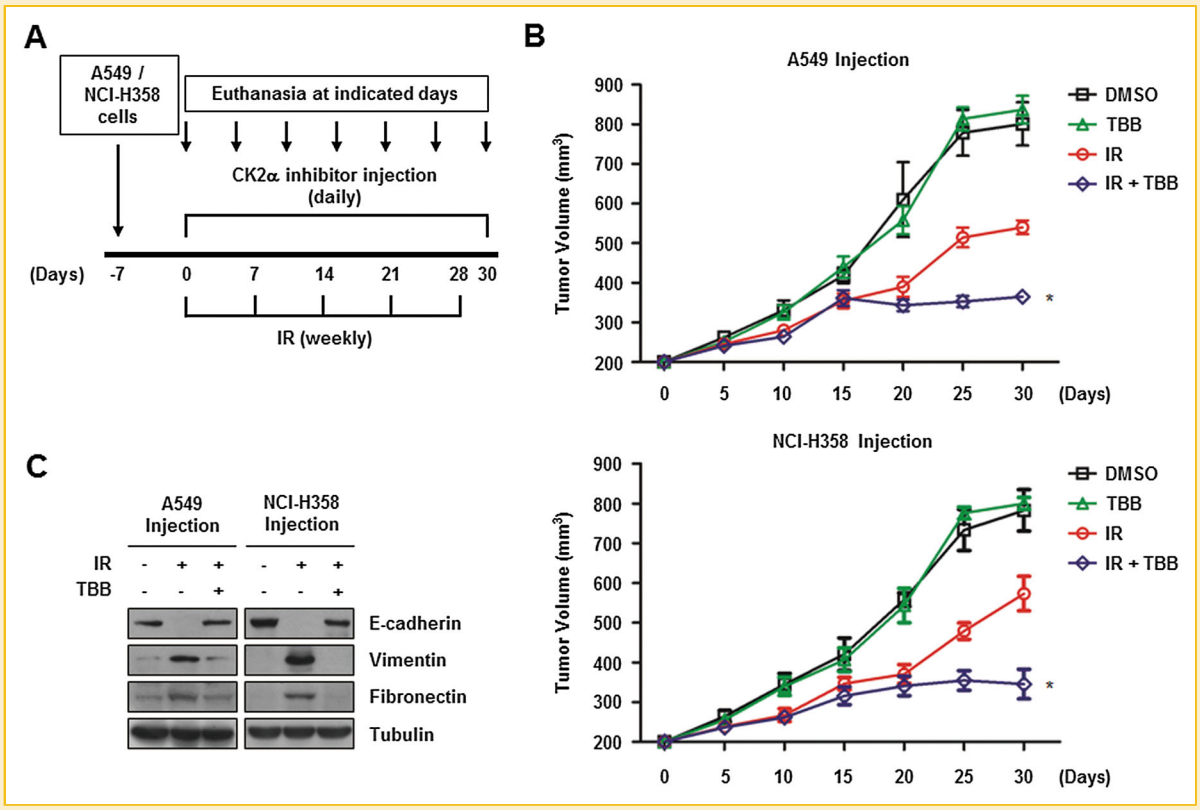

Fig. 6. Prevention of IR-induced MIF-rpS3 dissociation diminishes radioresistance and hinders EMT in vivo. (A) An experimental procedure for mouse xenograft models designed to investigate the *in vivo* radiosensitization effects of CK2α inhibition is presented. After verification of palpable tumor, BALB/c athymic nude mice (n = 3 per group) were irradiated at a dose of 10 Gy once a week for 4 week. Animals received DMSO or TBB (200 μg/kg body weight) intraperitoneally every day for 30 d. (B) The effects of a CK2α inhibitor on tumor volume of irradiated xenograft mouse models are indicated. $^{*}P < 0.05$ compared with tumor volume on day 30 in mice treated with irradiation alone. (C) The in vivo effects of a CK2α inhibitor on the expression levels of E-cadherin, Vimentin, and Fibronectin were measured by Western blot analysis.

by A549 cells) or 61.1% (for the group injected with NCI-H358 cells) on day 30 compared to mice that received radiation alone. Moreover, IR-induced expression of EMT-related proteins including Vimentin and Fibronectin was considerably decreased in the extracted tumor tissue lysates when TBB was directly administered at the tumor site in mice (Fig. 6C). Taken together, these findings suggest that the CK2α inhibitor significantly increased in vivo radiosensitization while inhibiting the EMT.

DISCUSSION

It has been demonstrated that IR can affect the microenvironment in which tumors reside [Barcellos-Hoff et al., 2005]. However, the roles of specific proteins in IR-dependent modification of cancer cells have not been thoroughly investigated to date. In the present study, we discovered that diminished MIF-rpS3 interaction caused by IR could be involved in tumors presenting aggressive phenotypes, suggesting that MIF, and rpS3 are prime candidates for controlling the metastatic capacity of tumors. The importance of environmental conditions on tumor development was suggested by the finding that IR-damaged stroma resulted in transplanted cancer cells encountering lower incidence of angiogenesis [Yoshimura et al., 2013]. Subsequent development of hypoxia could further elevate the aggressiveness of surviving tumor cells [Monnier et al., 2008]. Consequently, the small numbers of cancer cells that withstand radiotherapy could acquire aggressive metastatic phenotypes accompanied by poor prognoses. Consistently, a tumor bed effect (TBE) presenting decreased growth with highly metastatic properties of pre-irradiation site-embedded tumors has been reported [Rofstad et al., 2005]. Considering that mRNA and protein levels of MIF are increased under hypoxic conditions and MIF expression is elevated in cells localized near blood vessels [Bacher et al., 2003], one could surmise that MIF affects tumors exhibiting a TBE. It is plausible that MIF can play a deterministic role in causing IR-irradiated microenvironment to be metastatic. Thus, MIF could be a key factor in IR-induced metastasis.

Our results indicated that MIF and rpS3 have a physical association under unirradiated conditions. IR-dependent dissociation of this complex induced inflammation, proliferation, and metastasis of cancer cells. In an attempt to account for the action of dissociated MIF, we took note of our ITC data (Fig. 1) in which MIF interacted with rpS3 in its monomeric state. Although the crystal structure of MIF was homotrimer with two α-helices and a four-stranded β-sheet of each monomer constituting the center channel, it could also form monomers, dimers, and trimers at physiological

concentrations [Sun et al., 1996; Mischke et al., 1998]. A better understanding of MIF function may be attained by investigating what could regulate the structural characteristics of the protein. A previous study demonstrated the roles of C-terminal residues of MIF in the formation of a trimeric structure [Sugimoto et al., 1996]. On the other hand, mutation of Cys60 to Ser (C60S) led to increased formation of the MIF monomer [Mischke et al., 1998]. Intriguingly, MIF has thiol-protein oxidoreductase (TPOR) activity, which is mediated by Cys57-Ala58-Leu59-Cys60 (CALC) [Mischke et al., 1998]. The C60S mutant was shown to lack this oxidoreductase activity, and the disulfide bridge formed by Cys57 and Cys60 is known to be important in eliciting the catalytic activity. Therefore, the C60S mutant indicated that an increased proportion of MIF monomer coincides with the decreased oxidoreductase activity. Another report suggested that TPOR activity of MIF could be involved in its intracellular and immunological functions [Nguyen et al., 2003]. A 16-amino acid peptide containing the Phe50 to Ile65 residues of MIF interacts with Jab1, induces Erk1/2 phosphorylation, and elevates immunostimulatory effects analogously to the full-length MIF. Thus, it could be assumed that rpS3-bound monomeric MIF possesses diminished cellular activity. Moreover, it was proposed that the conformation of MIF should be modified during the enzymatic action since MIF shows little structural similarity to members of the TPOR family of proteins [Nguyen et al., 2003]. Based on our ITC data and reported structure, it is likely that IR-dissociated MIF undergoes changes in its oligomerization states to produce increased pro-inflammatory responses through CALC motif-activated TPOR activity.

According to our data, NF-κB activation was induced by decreased MIF-rpS3 interaction in response to IR. Dissociation of MIF and rpS3 did not occur in HA-rpS3 (T221A) which was not phosphorylated by CK2α (Fig. 2). Thus, Thr221 phosphorylation of rpS3 by CK2α is sufficient for dissociation of MIF-rpS3 complex and NF-κB activation in IR-irradiated NSCLC cells. It was known that both cell migration and EMT decrease with reduced CK2α expression in hepatocellular carcinoma cells [Wu et al., 2014]. Moreover, CK2α itself activates the NF-κB signaling pathway [Brown et al., 2010]. This could lead to the speculation that CK2α is an important regulator of IR-induced aggressiveness and metastatic properties of tumors indicated in our data. Nevertheless, we showed that NF-κB activation was attributed to MIF and rpS3, not CK2α, by demonstrating that knockdown of MIF expression sufficiently blocked IR-induced NF-κB activation and T221A rpS3 mimicked effects of CK2α siRNA (Fig. 3).

Our previous study demonstrated that rpS3 phosphorylation by CK2α under IR-given conditions occurs in radioresistant cells [Kim et al., 2013]. Phosphorylation of rpS3, dissociation of the complex between TNF receptor-associated factor 2 and rpS3, and activation of the NF-κB signaling pathway are not induced by IR in radiosensitive NSCLC cells. The cell lines used in the present study, A549, and NCI-H358, are known to possess considerable resistance to irradiation [Das et al., 2006]. We found that CK2α-mediated rpS3 phosphorylation by IR and subsequent dissociation of the MIF-rpS3 complex resulted in NF-κB activation. These findings indicate that rpS3 plays a major role in controlling post-IR modifications of cancer cells through two comparable but distinct circumstances. In a

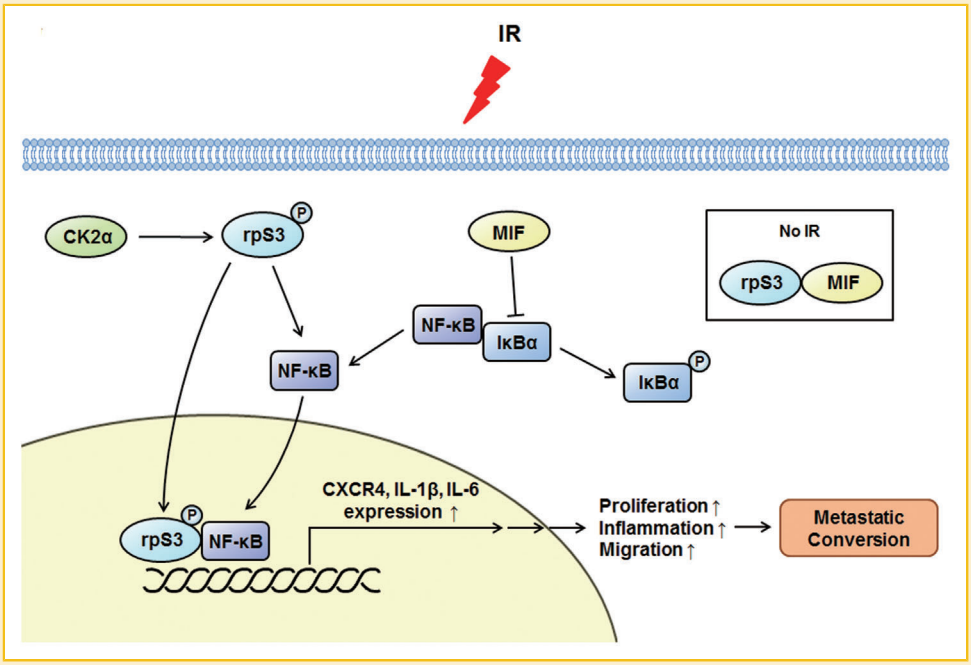

Fig. 7. A schematic diagram illustrates how dissociation of MIF-rpS3 complex induced by IR exposure leads to metastatic conversion of NSCLC. Under unirradiated conditions, MIF interacts with rpS3. However, IR mediates MIF-rpS3 complex dissociation by CK2α-induced phosphorylation of rpS3. Free form of MIF inhibits IκBα expression, which results in phosphorylation of the protein. Dissociated rpS3 binds NF-κB in the nucleus facilitating NF-κB activation. Increased expression of NF-κB target genes elevates inflammation, proliferation, and aggressiveness of NSCLC. A CK2α inhibitor, TBB could block dissociation of MIF and rpS3 to elicit in vitro and in vivo radiosensitization effects.

similar context, dissociation of homodomain-interacting protein kinase 2 (HIPK2) from wild-type p53-induced phosphatase 1 (WIP1) suggests another post-irradiation alteration [Choi et al., 2013]. Unlike HIPK2 phosphorylating WIP1 in unstressed cells, WIP1 phosphorylation is inhibited by disrupted HIPK2-WIP1 complex formation in irradiated cells, leading to WIP1 stabilization, and termination of the DNA double strand break-inducing pathways. These data indicate that phosphorylation of proteins and loss of protein–protein interactions may affect several events occurring in IR-irradiated cells.

One of the interactors of both MIF and rpS3, NM23-H1 is regarded as a suppressor of cancer metastasis [Jung et al., 2008; Youn et al., 2008]. This characteristic and our data indicates that NM23-H1 may be a factor that promotes NF-κB-induced inflammation and metastasis. Indeed, a recent study demonstrated that a variant of NM23-H1 inactivates NF-κB signaling by interacting with IκB kinase-β to suppress tumor metastasis [You et al., 2014]. MIF was also shown to interact with NM23-H1 through Cys60 of MIF and inhibit MIF-mediated suppression of p53 activity [Jung et al., 2008]. Based on pro-inflammatory effects of macrophages and on cancer growth exerted by MIF which suppresses the function of p53 [Bifulco et al., 2008], one could reason that the MIF-driven cancer cell proliferation, invasiveness, and metastasis in response to IR observed in our study were due to suppressed p53 activity. However, A549 cells contain wild-type p53 while NCI-H358 cells lack expression of p53 [Kasiappan et al., 2010; Osborne et al., 2014]. Similar results from the two cell lines in almost all of our experiments suggest that p53 was not associated with the results of the present study.

Undesired aggressiveness and metastasis of cancer cells have been obstacles of successful radiotherapy. The results of the present study indicated that MIF and rpS3 regulate IR-induced motility of NSCLC cells (Fig. 7). The activation of NF-κB was found to be mediated by the dissociation of MIF and rpS3 in response to IR. Expression of pro-inflammatory proteins was elevated, migration was increased, and EMT was promoted in irradiated NSCLC cells. In addition, in vivo radiosensitization and decreased metastatic characteristics were achieved through inhibition of CK2α that resulted in sustained MIF-rpS3 complex formation. Taken together, these findings suggest that MIF-rpS3 dissociation upon IR leading to NF-κB activation plays a significant role in inflammation, proliferation, and metastatic conversion. The results of the present study provide new insight that will be useful for efficiently treating NSCLC through targeting of MIF and rpS3 with pharmacologic agents in combination with radiotherapy.

ACKNOWLEDGMENTS

This work was supported by Radiation Technology R&D program through the National Research Foundation of Korea funded by the Ministry of Science, ICT & Future Planning (2013M2A2A7042502 to B Youn), a grant from the National R&D Program for Cancer Control, MOHW, Republic of Korea (1320100 to B Youn), Basic Science Research Program through the NRF funded by the MSIP (2014R1A1A1A05002112 to B Youn and NRF-2012R1A2A1A01009027 to J Kim), and Basic Science Research Program through the NRF funded by the MOE (2014R1A1A2004061 to H Youn). In addition, this work was supported by the Financial Supporting Project of Long-term Overseas Dispatch of PNU's Tenure-track Faculty, 2014 (to B Youn) and the 2014 Post-Doc. Development Program (to H Youn) of Pusan National University. The authors thank Dr. Chang-Deng Hu (Purdue University, West Lafayette, IN) and Dr. Ichi N. Maruyama (Okinawa Institute of Science and Technology Graduate University, Okinawa, Japan) for providing pBiFC-EGFR-VN and pBiFC-EGFR-VC constructs.

REFERENCES

Bacher M, Schrader J, Thompson N, Kuschela K, Gemsa D, Waeber G, Schlegel J. 2003. Up-regulation of macrophage migration inhibitory factor gene and protein expression in glial tumor cells during hypoxic and hypoglycemic stress indicates a critical role for angiogenesis in glioblastoma multiforme. Am J Pathol 162:11–17.

Barcellos-Hoff MH, Park C, Wright EG. 2005. Radiation and the microenvironment –tumorigenesis and therapy. Nat Rev Cancer 5:867–875.

Ben-Neriah Y, Karin M. 2011. Inflammation meets cancer, with NF-kappaB as the matchmaker. Nat Immunol 12:715–723.

Bifulco C, McDaniel K, Leng L, Bucala R. 2008. Tumor growth-promoting properties of macrophage migration inhibitory factor. Curr Pharm Des 14:3790–3801.

Bollrath J, Greten FR. 2009. IKK/NF-kappaB and STAT3 pathways: Central signalling hubs in inflammation-mediated tumour promotion and metastasis. EMBO Rep 10:1314–1319.

Bradley JD, Naqa I El, Drzymala RE, Trovo M, Jones G, Denning MD. 2010. Stereotactic body radiation therapy for early-stage non-small-cell lung cancer: The pattern of failure is distant. Int J Radiat Oncol Biol Phys 77:1146–1150.

Brown MS, Diallo OT, Hu M, Ehsanian R, Yang X, Arun P, Lu H, Korman V, Unger G, Ahmed K, Van Waes C, Chen Z. 2010. CK2 modulation of NF-kappaB, TP53, and the malignant phenotype in head and neck cancer by anti-CK2 oligonucleotides in vitro or in vivo via sub-50-nm nanocapsules. Clin Cancer Res 16:2295–2307.

Choi DW, Na W, Kabir MH, Yi E, Kwon S, Yeom J, Ahn JW, Choi HH, Lee Y, Seo KW, Shin MK, Park SH, Yoo HY, Isono K, Koseki H, Kim ST, Lee C, Kwon YK, Choi CY. 2013. WIP1, a homeostatic regulator of the DNA damage response, is targeted by HIPK2 for phosphorylation and degradation. Mol Cell 51:374–385.

Choudhary C, Kumar C, Gnad F, Nielsen ML, Rehman M, Walther TC, Olsen JV, Mann M. 2009. Lysine acetylation targets protein complexes and co-regulates major cellular functions. Science 325:834–840.

Das AK, Sato M, Story MD, Peyton M, Graves R, Redpath S, Girard L, Gazdar AF, Shay JW, Minna JD, Nirodi CS. 2006. Non-small-cell lung cancers with kinase domain mutations in the epidermal growth factor receptor are sensitive to ionizing radiation. Cancer Res 66:9601–9608.

Debnath J, Brugge JS. 2005. Modelling glandular epithelial cancers in three-dimensional cultures. Nat Rev Cancer 5:675–688.

Gamez-Pozo A, Sanchez-Navarro I, Calvo E, Agullo-Ortuno MT, Lopez-Vacas R, Diaz E, Camafeita E, Nistal M, Madero R, Espinosa E, Lopez JA, Fresno Vara JA. 2012. PTRF/cavin-1 and MIF proteins are identified as non-small cell lung cancer biomarkers by label-free proteomics. PLoS One 7:e3752.

Graifer D, Malygin A, Zharkov DO, Karpova G. 2014. Eukaryotic ribosomal protein S3: A constituent of translational machinery and an extraribosomal player in various cellular processes. Biochimie 99:8–18.

Grivennikov SI, Greten FR, Karin M. 2010. Immunity, inflammation, and cancer. Cell 140:883–899.

Gyrd-Hansen M, Meier P. 2010. IAPs: From caspase inhibitors to modulators of NF-kappaB, inflammation and cancer. Nat Rev Cancer 10:561–574.

Hou J, Aerts J, den Hamer B, van Ijcken W, den Bakker M, Riegman P, van der Leest C, van der Spek P, Foekens JA, Hoogsteden HC, Grosveld F, Philipsen S. 2010. Gene expression-based classification of non-small cell lung carcinomas and survival prediction. PLoS One 5:e10312.

Jang CY, Shin HS, Kim HD, Kim JW, Choi SY, Kim J. 2011. Ribosomal protein S3 is stabilized by sumoylation. Biochem Biophys Res Commun 414:523–527.

Jung H, Seong HA, Ha H. 2008. Direct interaction between NM23-H1 and macrophage migration inhibitory factor (MIF) is critical for alleviation of MIF-mediated suppression of p53 activity. J Biol Chem 283:32669–32679.

Kang J, Kim E, Kim W, Seong KM, Youn H, Kim JW, Kim J, Youn B. 2013. Rhamnetin and cirsiliol induce radiosensitization and inhibition of epithelial-mesenchymal transition (EMT) by miR-34a-mediated suppression of Notch-1 expression in non-small cell lung cancer cell lines. J Biol Chem 288:27343–27357.

Kasiappan R, Shih HJ, Wu MH, Choy C, Lin TD, Chen L, Hsu HL. 2010. The antagonism between MCT-1 and p53 affects the tumorigenic outcomes. Mol Cancer 9:311.

Kim E, Youn H, Kwon T, Son B, Kang J, Yang HJ, Seong KM, Kim W, Youn B. 2014. PAK1 tyrosine phosphorylation is required to induce epithelial-mesenchymal transition and radioresistance in lung cancer cells. Cancer Res 74:5520–5531.

Kim TS, Kim HD, Kim J. 2009. PKCdelta-dependent functional switch of rpS3 between translation and DNA repair. Biochim Biophys Acta 1793:395–405.

Kim W, Yang HJ, Youn H, Yun YJ, Seong KM, Youn B. 2010. Myricetin inhibits Akt survival signaling and induces Bad-mediated apoptosis in a low dose ultraviolet (UV)-B-irradiated HaCaT human immortalized keratinocytes. J Radiat Res 51:285–296.

Kim W, Youn H, Kwon T, Kang J, Kim E, Son B, Yang HJ, Jung Y, Youn B. 2013. PIM1 kinase inhibitors induce radiosensitization in non-small cell lung cancer cells. Pharmacol Res 70:90–101.

Kim W, Youn H, Seong KM, Yang HJ, Yun YJ, Kwon T, Kim YH, Lee JY, Jin YW, Youn B. 2011. PIM1-Activated PRAS40 Regulates Radioresistance in Non-small Cell Lung Cancer Cells through Interplay with FOXO3a, 14- 3–3 and Protein Phosphatases. Radiat Res 176:539–552.

Landi MT, Dracheva T, Rotunno M, Figueroa JD, Liu H, Dasgupta A, Mann FE, Fukuoka J, Hames M, Bergen AW, Murphy SE, Yang P, Pesatori AC, Consonni D, Bertazzi PA, Wacholder S, Shih JH, Caporaso NE, Jen J. 2008. Gene expression signature of cigarette smoking and its role in lung adenocarcinoma development and survival. PLoS One 3:e1651.

Leeming DJ, Bay-Jensen AC, Vassiliadis E, Larsen MR, Henriksen K, Karsdal MA. 2011. Post-translational modifications of the extracellular matrix are key events in cancer progression: Opportunities for biochemical marker development. Biomarkers 16:193–205.

Li F, Sethi G. 2010. Targeting transcription factor NF-kappaB to overcome chemoresistance and radioresistance in cancer therapy. Biochim Biophys Acta 1805:167–180.

Magne N, Toillon RA, Bottero V, Didelot C, Houtte PV, Gerard JP, Peyron JF. 2006. NF-kappaB modulation and ionizing radiation: mechanisms and future directions for cancer treatment. Cancer Lett 231:158–168.

Mischke R, Kleemann R, Brunner H, Bernhagen J. 1998. Cross-linking and mutational analysis of the oligomerization state of the cytokine macrophage migration inhibitory factor (MIF). FEBS Lett 427:85–90.

Monnier Y, Farmer P, Bieler G, Imaizumi N, Sengstag T, Alghisi GC, Stehle JC, Ciarloni L, Andrejevic-Blant S, Moeckli R, Mirimanoff RO, Goodman SL, Delorenzi M, Ruegg C. 2008. CYR61 and alphaVbeta5 integrin cooperate to promote invasion and metastasis of tumors growing in preirradiated stroma. Cancer Res 68:7323–7331.

Moritz A, Li Y, Guo A, Villen J, Wang Y, MacNeill J, Kornhauser J, Sprott K, Zhou J, Possemato A, Ren JM, Hornbeck P, Cantley LC, Gygi SP, Rush J, Comb MJ. 2010. Akt-RSK-S6 kinase signaling networks activated by oncogenic receptor tyrosine kinases. Sci Signal 3:ra64.

Nguyen MT, Beck J, Lue H, Funfzig H, Kleemann R, Koolwijk P, Kapurniotu A, Bernhagen J. 2003. A 16-residue peptide fragment of macrophage migration inhibitory factor, MIF-(50-65), exhibits redox activity and has MIF-like biological functions. J Biol Chem 278:33654–33671.

Osborne JK, Guerra ML, Gonzales JX, McMillan EA, Minna JD, Cobb MH. 2014. NeuroD1 mediates nicotine-induced migration and invasion via regulation of the nicotinic acetylcholine receptor subunits in a subset of neural and neuroendocrine carcinomas. Mol Biol Cell 25:1782–1792.

Powell JW, Dexter E, Scalzetti EM, Bogart JA. 2009. Treatment advances for medically inoperable non-small-cell lung cancer: Emphasis on prospective trials. Lancet Oncol 10:885–894.

Rendon BE, Roger T, Teneng I, Zhao M, Al-Abed Y, Calandra T, Mitchell RA. 2007. Regulation of human lung adenocarcinoma cell migration and invasion by macrophage migration inhibitory factor. J Biol Chem 282:29910–29918.

Rofstad EK, Mathiesen B, Henriksen K, Kindem K, Galappathi K. 2005. The tumor bed effect: Increased metastatic dissemination from hypoxia-induced up-regulation of metastasis-promoting gene products. Cancer Res 65:2387–2396.

Schafer T, Maco B, Petfalski E, Tollervey D, Bottcher B, Aebi U, Hurt E. 2006. Hrr25-dependent phosphorylation state regulates organization of the pre-40S subunit. Nature 441:651–655.

Sugimoto H, Suzuki M, Nakagawa A, Tanaka I, Nishihira J. 1996. Crystal structure of macrophage migration inhibitory factor from human lymphocyte at 2.1. A resolution. FEBS Lett 389:145–148.

Sun HW, Bernhagen J, Bucala R, Lolis E. 1996. Crystal structure at 2.6-A resolution of human macrophage migration inhibitory factor. Proc Natl Acad Sci U S A 93:5191–5196.

Wan F, Anderson DE, Barnitz RA, Snow A, Bidere N, Zheng L, Hegde V, Lam LT, Staudt LM, Levens D, Deutsch WA, Lenardo MJ. 2007. Ribosomal protein S3: A KH domain subunit in NF-kappaB complexes that mediates selective gene regulation. Cell 131:927–939.

White ES, Strom SR, Wys NL, Arenberg DA. 2001. Non-small cell lung cancer cells induce monocytes to increase expression of angiogenic activity. J Immunol 166:7549–7555.

Wu D, Sui C, Meng F, Tian X, Fu L, Li Y, Qi X, Cui H, Liu Y, Jiang Y. 2014. Stable knockdown of protein kinase CK2-alpha (CK2alpha) inhibits migration and invasion and induces inactivation of hedgehog signaling pathway in hepatocellular carcinoma Hep G2 cells. Acta Histochem 116:1501–1508.

Yang HJ, Youn H, Seong KM, Jin YW, Kim J, Youn B. 2013. Phosphorylation of Ribosomal Protein S3 and Antiapoptotic TRAF2 Protein Mediates Radioresistance in Non-small Cell Lung Cancer Cells. J Biol Chem 288:2965–2975.

Yang HJ, Youn H, Seong KM, Yun YJ, Kim W, Kim YH, Lee JY, Kim CS, Jin YW, Youn B. 2011. Psoralidin, a dual inhibitor of COX-2 and 5-LOX, regulates ionizing radiation (IR)-induced pulmonary inflammation. Biochem Pharmacol 82:524–534.

Yoshimura M, Itasaka S, Harada H, Hiraoka M. 2013. Microenvironment and radiation therapy. Biomed Res Int 2013:685308.

You DJ, Park CR, Lee HB, Moon MJ, Kang JH, Lee C, Oh SH, Ahn C, Seong JY, Hwang JI. 2014. A splicing variant of NME1 negatively regulates NF-kappaB signaling and inhibits cancer metastasis by interacting with IKKbeta. J Biol Chem 289:17709–17720.

Youn B, Kim HD, Kim J. 2008. Nm23-H1/nucleoside diphosphate kinase as a key molecule in breast tumor angiogenesis. Expert Opin Ther Targets 12:1419–1430.

SUPPORTING INFORMATION

Additional supporting information may be found in the online version of this article at the publisher's web-site